


 Cite this: *RSC Adv.*, 2021, **11**, 23597

## A novel coumarin-based colorimetric and fluorescent probe for detecting increasing concentrations of $\text{Hg}^{2+}$ *in vitro* and *in vivo*<sup>†</sup>

 Li Huang,<sup>a</sup> Wenlong Sheng,<sup>b</sup> Lizhen Wang,<sup>b</sup> Xia Meng,<sup>b</sup> Hongdong Duan<sup>a</sup> <sup>✉</sup> and Liqun Chi<sup>\*c</sup>

Mercury has complex biological toxicity and can cause a variety of physiological diseases and even death, so it is of great importance to develop novel strategies for detecting trace mercury in environmental and biological samples. In this work, we designed a new coumarin-based colorimetric and fluorescent probe CNS, which could be obtained from inexpensive starting materials with high overall yield in three steps. Probe CNS could selectively respond to  $\text{Hg}^{2+}$  with obvious color and fluorescence changes, and the presence of other metal ions had no effect on the fluorescence changes. Probe CNS also exhibited high sensitivity against  $\text{Hg}^{2+}$ , with a detection limit as low as  $2.78 \times 10^{-8}$  M. More importantly, the behavioral tracks of zebrafish had no obvious changes upon treatment with 10  $\mu\text{M}$  probe CNS, thus indicating its low toxicity. The probe showed potential application value and was successfully used for detecting  $\text{Hg}^{2+}$  in a test strip, HeLa cells and living zebrafish larvae.

Received 21st February 2021

Accepted 25th June 2021

DOI: 10.1039/d1ra01408k

[rsc.li/rsc-advances](http://rsc.li/rsc-advances)

### 1. Introduction

Mercury (Hg) is one of the most toxic heavy-metal ions in the environment and has attracted increasing attention due to its accumulation in natural ecosystems.<sup>2–4</sup> Generally, mercury exists as elemental mercury, oxidized mercury ( $\text{Hg}^{2+}$ ) and mercury particles in air, soil and water.<sup>5–7</sup> All these mercury species are not biodegradable and can be concentrated in the human body, thereby causing irreversible damage to the liver, kidneys, brain, and endocrine and central nervous systems.<sup>8–11</sup> In particular,  $\text{Hg}^{2+}$  can be easily converted into the lipophilic methyl mercury, which exhibits good membrane penetrating ability and can be easily absorbed by aquatic organisms.<sup>12–14</sup> Recently, mercury chloride and methyl mercury have been classified as potentially carcinogenic agents by the Environmental Protection Agency.<sup>9</sup> Therefore, development of novel strategies for selectively and sensitively detecting trace mercury in environmental and biological samples is of great importance.

Several methods have been developed for detecting mercury species, such as atomic absorption–emission spectrometry,<sup>15,16</sup> inductively coupled plasma-atomic emission spectrometry,<sup>17</sup> and anodic stripping voltammetry.<sup>18</sup> However, these methods

always suffer from complicated manipulation procedure and expensive instrumentation.<sup>1,14</sup> In contrast, fluorescent probes have attracted increasing attention because of their low cost, high sensitivity and selectivity, noninvasiveness, and experimental convenience.<sup>19–22</sup> In the past several years, great efforts have been made on the development of fluorescent probes for mercury ions based on the heteroatom-based coordination reaction, and  $\text{Hg}^{2+}$ -promoted elimination and desulfurization reactions.<sup>23–33</sup> A portion of them exhibit excellent selectivity and sensitivity, fast response time, and low detection limits. However, these reported fluorescent probes still have limitations including complex synthesis routine, using expensive chemical reagents, high toxicity, and poor biocompatibility, thus being not applicable for detecting  $\text{Hg}^{2+}$  in biological systems and environmental samples.

Coumarin is a well-known secondary metabolite found in different parts of plants.<sup>34</sup> Structural modification of coumarin can afford various derivatives with various pharmacological activities and low toxicity to human body.<sup>35</sup> Some of these coumarin derivatives exhibit strong fluorescent emission and can be used as fluorescent probes for imaging different metal ions and metabolites in living biological systems.<sup>35,36</sup> Coumarin derivatives can also be used as fluorescent tags or imaging agents for discriminating tumor lesions and investigating the subcellular localization of drugs.<sup>37–46</sup> In our research, a novel intramolecular charge transfer (ICT)-based fluorescent probe CNS (Scheme 1), employing coumarin as the fluorophore and thioacetals as the reacting site for  $\text{Hg}^{2+}$ , was constructed by a facile and highly efficient synthesis strategy. The probe should be highly selective and sensitive to  $\text{Hg}^{2+}$ , because the electron-rich dithioacetal group can be specifically and rapidly cleaved in the presence of  $\text{Hg}^{2+}$ . The optical

<sup>a</sup>School of Chemistry and Chemical Engineering, Qilu University of Technology (Shandong Academy of Sciences), Jinan 250353, PR China. E-mail: hdduan67@163.com

<sup>b</sup>Biology Institute, Qilu University of Technology (Shandong Academy of Sciences), Jinan 250014, Shandong Province, China

<sup>c</sup>Department of Pharmacy, Haidian Maternal & Child Health Hospital of Beijing, Beijing, 100080, PR China. E-mail: chilqun@sohu.com

<sup>†</sup> Electronic supplementary information (ESI) available. See DOI: 10.1039/d1ra01408k



properties and probing behaviors of CNS against  $\text{Hg}^{2+}$ , and its applications in living cells and zebrafish were investigated.

## 2. Experimental

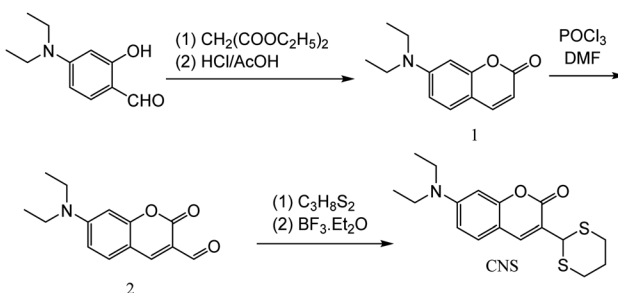
### 2.1 Materials and measurements

All chemical reagents were obtained commercially and used without further purification.  $^1\text{H}$  NMR and  $^{13}\text{C}$  NMR spectra were recorded on a Bruker AV-400 spectrometer using TMS as internal standard. Electrospray ionization (ESI) mass spectra were recorded by an LC-MS 2010A (Shimadzu) instrument. The high-resolution mass spectrum (HRMS) was measured using a Q-TOF6510 spectrograph (Agilent). The UV-vis absorption spectra were analyzed by a UV-2600 PC spectrophotometer (Shimadzu, Japan). The fluorescence spectra were recorded on a F-7000 Fluorescence Spectrophotometer (Hitachi, Japan).

### 2.2 Synthesis of probe CNS

**2.2.1 Synthesis of compound 1.** To a solution of 4-diethylaminosalicylaldehyde (3.86 g, 20 mmol) in ethyl alcohol (120 mL) was added diethyl malonate (7 mL, 25 mmol), piperidine (2.0 mL, 0.02 mmol) and two drops of acetic acid. The reaction was heated to reflux and stirred for 6 h. Then all volatiles were evaporated under reduced pressure, and then concentrated. HCl (40 mL) and acetic acid (40 mL) were added and the reaction was continued at 110 °C temperature for 24 h. This solution was cooled to room temperature and poured into ice water (150 mL). NaOH solution (30%) was added dropwise to adjust the pH to 6, and a brown precipitate formed immediately. After stirring for 1 h, the mixture was filtered, washed with water, purified through a flash silica gel column by the using DCM as eluent to afford compound 1.  $^1\text{H}$  NMR (400 MHz,  $\text{DMSO}-d_6$ )  $\delta$  7.69 (d,  $J = 9.3$  Hz, 1H), 7.29 (d,  $J = 8.8$  Hz, 1H), 6.55 (dd,  $J = 8.8, 2.5$  Hz, 1H), 6.38 (d,  $J = 2.4$  Hz, 1H), 5.85 (d,  $J = 9.3$  Hz, 1H), 3.29 (q,  $J = 7.0$  Hz, 4H), 0.98 (t,  $J = 7.0$  Hz, 6H) (Fig. S1†).

**2.2.2 Synthesis of compound 2.** Dry DMF (3 mL) was added dropwise to  $\text{POCl}_3$  (3 mL) 0 °C, the mixture was stirred for 10 min and slowly added to a solution of 1 (2.17 g, 10 mmol) in dry DMF (20 mL). The resulting mixture was stirred at 60 °C for 24 h and then poured into ice water (150 mL). NaOH solution (30%) was added to adjust the pH to 7, and a large amount of precipitate was formed. The mixture was filtered and thoroughly washed with water, purified through a flash silica gel column to give compound 2 as an orange solid.  $^1\text{H}$  NMR (400



Scheme 1 Synthesis step of probe CNS.

MHz,  $\text{DMSO}-d_6$ )  $\delta$  9.77 (s, 1H), 8.29 (s, 1H), 7.56 (d,  $J = 9.0$  Hz, 1H), 6.70 (dd,  $J = 9.0, 2.4$  Hz, 1H), 6.48 (d,  $J = 2.4$  Hz, 1H), 3.38 (q,  $J = 7.1$  Hz, 4H), 1.02 (t,  $J = 7.0$  Hz, 6H), 0.13 (s, 3H) (Fig. S2†).

**2.2.3 Synthesis of CNS.** Compound 2 (0.245 g, 1 mmol) was added to a 100 mL three-necked flask and dissolved in 20 mL ethyl alcohol. Then, to the mixture was added propane-1,3-dithiol (0.1 mL, 0.99 mmol) followed by a catalytic amount of  $\text{BF}_3\cdot\text{Et}_2\text{O}$ . The reaction was heated to reflux and stirred for 2 h. The resulting mixture was cooled to room temperature and refrigerated for 30 minutes. The solvent was evaporated and the crude product was recrystallized by ethyl alcohol to afford CNS as a pale yellow solid (0.311 g, 75.05% for three steps).  $^1\text{H}$  NMR (400 MHz,  $\text{DMSO}-d_6$ )  $\delta$  7.94 (s, 1H), 7.55 (d,  $J = 8.9$  Hz, 1H), 6.71 (dd,  $J = 8.9, 2.5$  Hz, 1H), 6.52 (d,  $J = 2.4$  Hz, 1H), 5.35 (s, 1H), 3.44 (q,  $J = 7.0$  Hz, 4H), 3.11 (ddd,  $J = 14.6, 12.3, 2.3$  Hz, 2H), 2.89 (dt,  $J = 14.0, 3.7$  Hz, 2H), 2.12 (ddd,  $J = 14.0, 4.5, 2.3$  Hz, 1H), 1.79–1.52 (m, 1H), 1.12 (t,  $J = 7.0$  Hz, 6H) (Fig. S3†).  $^{13}\text{C}$  NMR (101 MHz,  $\text{DMSO}-d_6$ )  $\delta$  156.11, 151.31, 142.59, 130.16, 118.40, 109.69, 107.96, 96.71, 44.57, 43.31, 31.52, 25.23, 12.74 (Fig. S4†). HRMS (ESI): calcd for  $\text{C}_{17}\text{H}_{21}\text{NO}_2\text{S}_2$ : 335.1014, found: 336.1157 for  $[\text{M} + \text{H}]^+$  (Fig. S5†).

### 2.3 Preparation of stock solutions

The CNS (3.51 mg, 1.0 mmol) was dissolved in THF and the volume was set to 100 mL to give the probe stock solution ( $1.0 \times 10^{-3}$  M). The stock solutions of the metal ions with the concentration of  $1.0 \times 10^{-3}$  M were prepared by dissolving 1.0 mmol of each inorganic salt ( $\text{AgNO}_3$ ,  $\text{Ba}(\text{NO}_3)_2$ ,  $\text{Cd}(\text{NO}_3)_2 \cdot 4\text{H}_2\text{O}$ ,  $\text{Co}(\text{NO}_3)_2 \cdot 6\text{H}_2\text{O}$ ,  $\text{Cu}(\text{NO}_3)_2 \cdot 3\text{H}_2\text{O}$ ,  $\text{FeSO}_4 \cdot 7\text{H}_2\text{O}$ ,  $\text{Fe}(\text{NO}_3)_3 \cdot 9\text{H}_2\text{O}$ ,  $\text{Hg}(\text{NO}_3)_2 \cdot \text{H}_2\text{O}$ ,  $\text{KNO}_3$ ,  $\text{NaNO}_3$ ,  $\text{Ni}(\text{NO}_3)_2 \cdot 6\text{H}_2\text{O}$ ,  $\text{Pb}(\text{NO}_3)_2$ ,  $\text{Sr}(\text{NO}_3)_2$ ,  $\text{Zn}(\text{NO}_3)_2 \cdot 6\text{H}_2\text{O}$ ) in water and the volume was set to 100 mL.

### 2.4 The UV-vis absorption spectra of CNS in the presence of different metal ions

The solution of CNS (1 mL) was placed in a 100 mL volumetric flask, and added 1.0 equiv. metal ions ( $\text{Ag}^+$ ,  $\text{Ba}^{2+}$ ,  $\text{Cu}^{2+}$ ,  $\text{Co}^{2+}$ ,  $\text{Cd}^{2+}$ ,  $\text{Fe}^{3+}$ ,

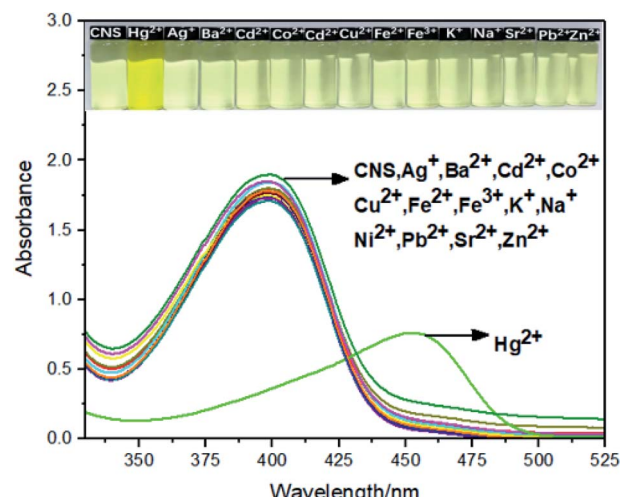


Fig. 1 The absorption spectra of CNS upon addition of various metal ions in  $\text{THF}/\text{H}_2\text{O}$  (1 : 1, V/V) solution ( $1.0 \times 10^{-5}$  M). Inset: The photograph of CNS solution ( $1.0 \times 10^{-5}$  M) in the presence of  $1.0 \times 10^{-5}$  M of  $\text{Hg}^{2+}$ .



$\text{Fe}^{2+}$ ,  $\text{K}^+$ ,  $\text{Na}^+$ ,  $\text{Ni}^{2+}$ ,  $\text{Pb}^{2+}$ ,  $\text{Sr}^{2+}$ ,  $\text{Zn}^{2+}$  and  $\text{Hg}^{2+}$ ), constant to 100 mL with  $\text{THF}/\text{H}_2\text{O}$  (1 : 1, v/v) solution, then get the  $1.0 \times 10^{-5}$  M fluid to be tested. The fluid to be tested were added to the quartz cell, and the corresponding ultraviolet spectrum was measured.

## 2.5 The fluorescence spectra of CNS in the presence of different metal ions

The solution of CNS (1 mL) was placed in a 100 mL volumetric flask, and added 1.0 equiv. metal ions ( $\text{Ag}^+$ ,  $\text{Ba}^{2+}$ ,  $\text{Cu}^{2+}$ ,  $\text{Co}^{2+}$ ,  $\text{Cd}^{2+}$ ,  $\text{Fe}^{3+}$ ,  $\text{Fe}^{2+}$ ,  $\text{K}^+$ ,  $\text{Na}^+$ ,  $\text{Ni}^{2+}$ ,  $\text{Pb}^{2+}$ ,  $\text{Sr}^{2+}$ ,  $\text{Zn}^{2+}$  and  $\text{Hg}^{2+}$ ), constant to 100 mL with  $\text{THF}/\text{H}_2\text{O}$  (1 : 1, v/v) solution, then get the  $1.0 \times 10^{-5}$  M fluid to be tested. The fluid to be tested were added to the quartz cell, and the corresponding fluorescence spectrum was measured.

## 2.6 Competition experiments

The solution of CNS (1 mL) was placed in a 100 mL volumetric flask, 1 mL  $\text{Hg}^{2+}$  was added to the volumetric flask, and then added 1.0 equiv. other metal ions ( $\text{Ag}^+$ ,  $\text{Ba}^{2+}$ ,  $\text{Cu}^{2+}$ ,  $\text{Co}^{2+}$ ,  $\text{Cd}^{2+}$ ,  $\text{Fe}^{3+}$ ,

$\text{Fe}^{2+}$ ,  $\text{K}^+$ ,  $\text{Na}^+$ ,  $\text{Ni}^{2+}$ ,  $\text{Pb}^{2+}$ ,  $\text{Sr}^{2+}$ ,  $\text{Zn}^{2+}$ ), constant to 100 mL with  $\text{THF}/\text{H}_2\text{O}$  (1 : 1, v/v) solution. The fluid to be tested were added to the quartz cell, and the fluorescence spectrum was measured.

## 2.7 Cell culture and fluorescence imaging

HeLa cells were grown in Dulbecco's Modified Eagle Medium (DMEM) containing 10% fetal bovine serum (FBS) and 1% penicillin-streptomycin. After incubating at 37 °C in a humidified atmosphere with 5%  $\text{CO}_2$  for 24 h, cells were washed with PBS buffer (phosphate buffered saline, pH = 7.2) and incubated with fresh medium containing 10  $\mu\text{M}$  probe CNS for 30 min. Then, cells were treated with different concentrations of  $\text{Hg}^{2+}$  (0, 10, 20, and 50  $\mu\text{M}$ ) for 10 min and the fluorescence spectra were measured on a laser confocal microscopy (Olympus, Japan). For the control group, HeLa cells were grown in DMEM for 30 min without any treatment.

## 2.8 Zebrafish maintenance and fluorescence imaging

The wild type zebrafish eggs were grown in 24-well plate with E3 water containing 0.2 mM 2-phenylthiourea. After incubating in

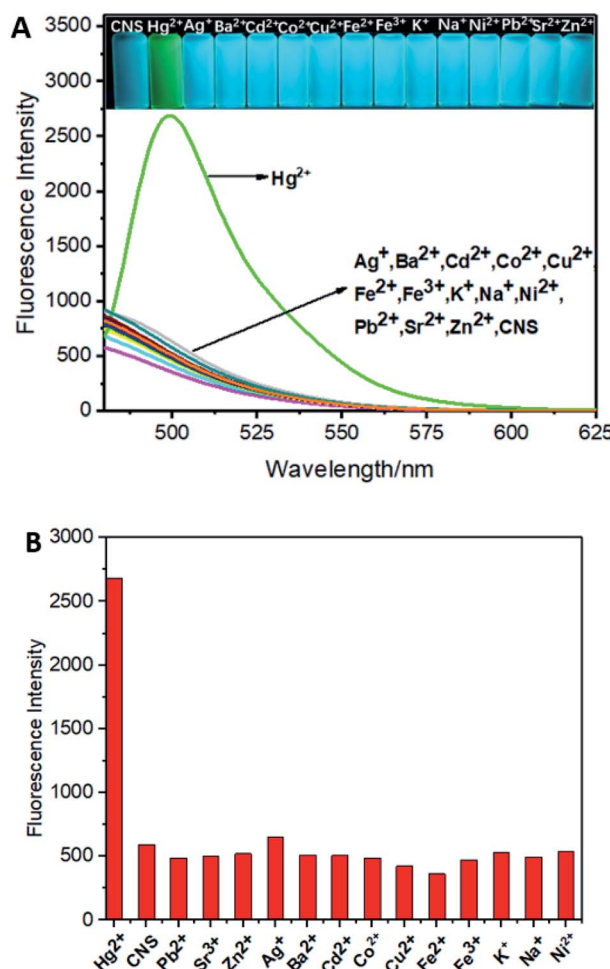


Fig. 2 (A) The fluorescence spectra of CNS upon addition of various metal ions in  $\text{THF}/\text{H}_2\text{O}$  (1 : 1, V/V) solution ( $1.0 \times 10^{-5}$  M). (B) Comparison of  $\text{Hg}^{2+}$  and other metal ions detected by probe CNS. Inset: The photograph of CNS solution ( $1.0 \times 10^{-5}$  M) in the presence of  $1.0 \times 10^{-5}$  M  $\text{Hg}^{2+}$  under the UV light. Excitation wavelength = 460 nm.

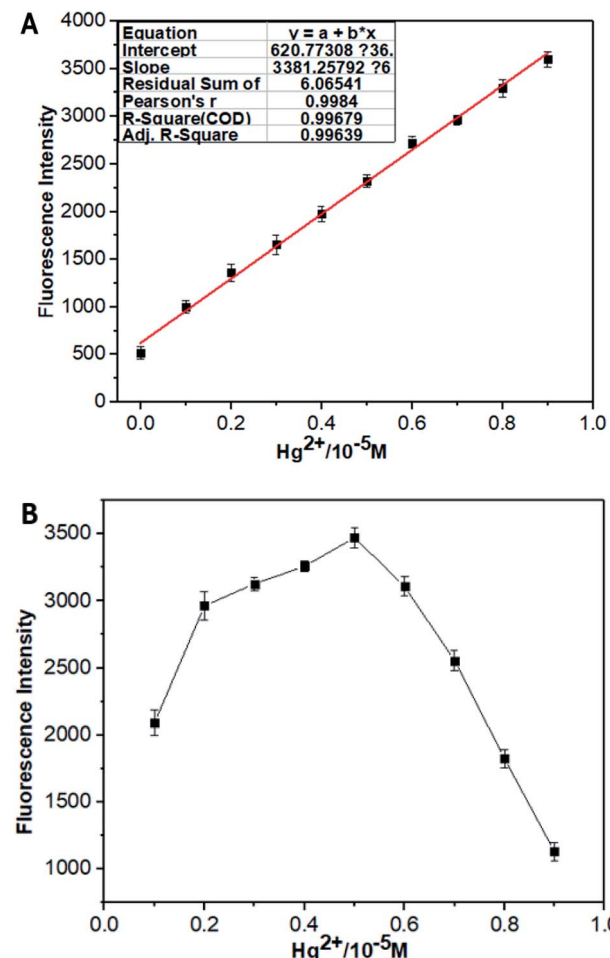
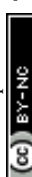


Fig. 3 (A) The relative fluorescence intensity of CNS  $\text{THF}/\text{H}_2\text{O}$  solution ( $10^{-5}$  M, 1 : 1, V/V) as a function of  $\text{Hg}^{2+}$  concentration in the range of  $1 \times 10^{-6}$  to  $1 \times 10^{-5}$  M. (B) Job's plot of CNS with  $\text{Hg}^{2+}$  ( $[\text{CNS}] + [\text{Hg}^{2+}] = 10$  M),  $\text{THF}/\text{H}_2\text{O}$  (1 : 1, V/V) solution ( $1.0 \times 10^{-5}$  M). Excitation wavelength = 460 nm.



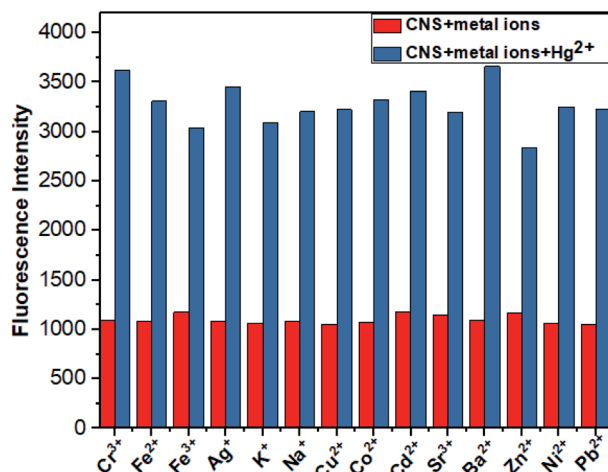


Fig. 4 Competitive tests for Hg detection by probe **CNS**. Red indicates probe detection of other metal ions, blue indicates probe detection of **CNS** + other metal ions +  $\text{Hg}^{2+}$ , THF/H<sub>2</sub>O solution (10<sup>-5</sup> M, 1 : 1, V/V). Excitation wavelength = 460 nm.

a light incubator at 28 ± 0.5 °C for 5 days, the zebrafish larvae were treated with new medium containing 10 μM probe **CNS** for 30 min. Then, different concentrations of  $\text{Hg}^{2+}$  (0, 5, 10, and 20 μM) were added to the medium, and the fluorescence spectra were measured on a laser confocal microscopy after 10 min of incubation. For the control group, the zebrafish larvae were grown in E3 water for 30 min without any treatment. The toxicity of probe **CNS** was measured using 5 days zebrafish larvae. Zebrafish larvae were treated with E3 water containing different concentrations of **CNS** (0, 5, and 10 μM) for 24 h, and the behavioral tracks of zebrafish were analyzed on an automated computerized video-tracking system (Viewpoint, Lyon, France).

### 3. Results and discussion

#### 3.1 Selective recognition of $\text{Hg}^{2+}$

The absorption spectra of probe **CNS** under the influence of various metal ions ( $\text{Ag}^+$ ,  $\text{Ba}^{2+}$ ,  $\text{Cu}^{2+}$ ,  $\text{Co}^{2+}$ ,  $\text{Cd}^{2+}$ ,  $\text{Fe}^{3+}$ ,  $\text{Fe}^{2+}$ ,  $\text{K}^+$ ,  $\text{Na}^+$ ,  $\text{Ni}^{2+}$ ,  $\text{Pb}^{2+}$ ,  $\text{Sr}^{2+}$ ,  $\text{Zn}^{2+}$  and  $\text{Hg}^{2+}$ ) were investigated in THF/H<sub>2</sub>O (1 : 1, V/V) solution (1.0 × 10<sup>-5</sup> M), and the results were depicted in Fig. 1. The free probe **CNS** exhibited a strong absorption peak centered at 395 nm, which was shifted to 459 nm after adding 2.0 × 10<sup>-5</sup> M  $\text{Hg}^{2+}$  ions. In contrast, addition of other metal ions ( $\text{Ag}^+$ ,  $\text{Ba}^{2+}$ ,  $\text{Cu}^{2+}$ ,  $\text{Co}^{2+}$ ,  $\text{Cd}^{2+}$ ,  $\text{Fe}^{3+}$ ,  $\text{Fe}^{2+}$ ,  $\text{K}^+$ ,  $\text{Na}^+$ ,  $\text{Ni}^{2+}$ ,  $\text{Pb}^{2+}$ ,  $\text{Sr}^{2+}$ ,  $\text{Zn}^{2+}$  and  $\text{Hg}^{2+}$ ) showed no effect on the absorption spectrum of **CNS** at the same concentration and under analogous test conditions. In addition, the probe solution turns yellow after adding  $\text{Hg}^{2+}$ , while adding other metal ions induced no obvious color changes.

The fluorescence spectra of probe **CNS** upon treatment of various metal ions including  $\text{Ag}^+$ ,  $\text{Ba}^{2+}$ ,  $\text{Cu}^{2+}$ ,  $\text{Co}^{2+}$ ,  $\text{Cd}^{2+}$ ,  $\text{Fe}^{3+}$ ,  $\text{Fe}^{2+}$ ,  $\text{K}^+$ ,  $\text{Na}^+$ ,  $\text{Ni}^{2+}$ ,  $\text{Pb}^{2+}$ ,  $\text{Sr}^{2+}$ ,  $\text{Zn}^{2+}$  and  $\text{Hg}^{2+}$  were tested in THF/H<sub>2</sub>O (1 : 1, V/V) solution (1.0 × 10<sup>-5</sup> M). As shown in Fig. 2A, addition of  $\text{Hg}^{2+}$  ion to the solution of **CNS** in THF/H<sub>2</sub>O resulted in obvious fluorescence improvement and the maximum emission wavelength was 505 nm, whereas adding other metal ions resulted in negligible fluorescence

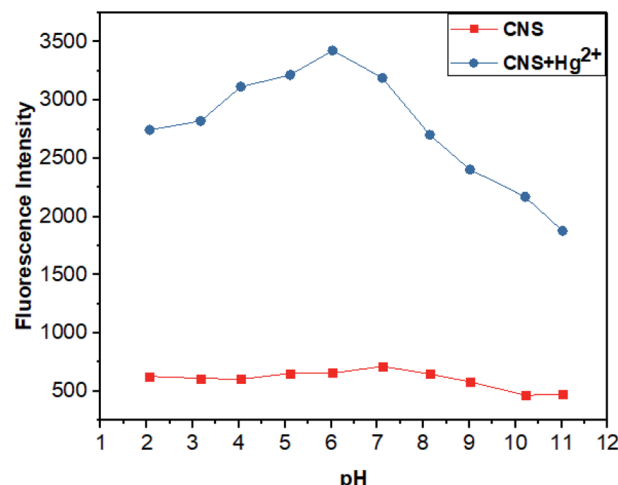


Fig. 5 Fluorescence intensity of probe **CNS** (10<sup>-5</sup> M) and **CNS** +  $\text{Hg}^{2+}$  (10<sup>-5</sup> M) at different pH, <sup>2-11</sup> THF/H<sub>2</sub>O solution (1 : 1, V/V). Excitation wavelength = 460 nm.

improvement Fig. 2B. These results indicated the high selectivity of **CNS** toward  $\text{Hg}^{2+}$  over other tested metal ions.

#### 3.2 Sensitivity studies

The fluorescence titration experiments of **CNS** in THF/H<sub>2</sub>O (1 : 1, V/V) solution (1.0 × 10<sup>-5</sup> M) against increasing concentrations of  $\text{Hg}^{2+}$  was carried out to investigate the fluorescence change of **CNS** under the influence of  $\text{Hg}^{2+}$ . As depicted in Fig. 3A, probe **CNS** showed almost no fluorescence in THF/H<sub>2</sub>O (1 : 1, V/V) solution (1.0 × 10<sup>-5</sup> M). After adding increasing concentrations of  $\text{Hg}^{2+}$  (0–14 μM), a significant fluorescence improvement could be observed around 505 nm, and the fluorescence intensity become stable when the concentration of  $\text{Hg}^{2+}$  was above 4 μM. These results proved the 1 : 1 response of probe **CNS** to  $\text{Hg}^{2+}$ . The Job's plot of probe **CNS** with  $\text{Hg}^{2+}$  was further investigated in THF/H<sub>2</sub>O (1 : 1, V/V).

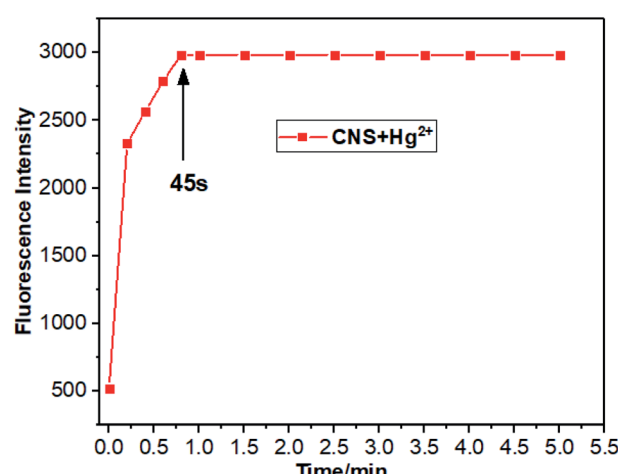


Fig. 6 Response time and stability of probe **CNS**. Fluorescence intensity of **CNS** +  $\text{Hg}^{2+}$  (10<sup>-5</sup> M), THF/H<sub>2</sub>O solution (1 : 1, V/V). Excitation wavelength = 460 nm.



V) solution ( $1.0 \times 10^{-5}$  M), and the result was shown in Fig. 3B. The maximum fluorescence intensity was detected to be 0.5 (molar fraction of  $[\text{Hg}^{2+}]/[\text{CNS} + \text{Hg}^{2+}]$ ), which proved a 1 : 1 stoichiometry for the reaction of probe CNS with  $\text{Hg}^{2+}$ .

### 3.3 Competition experiments

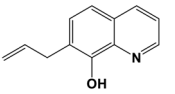
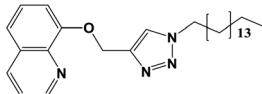
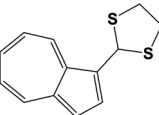
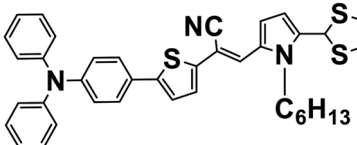
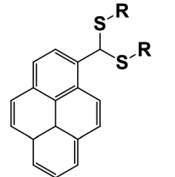
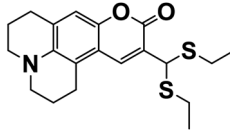
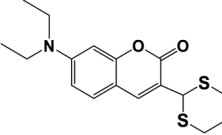
It is very necessary to study the anti-interference of probe CNS, as various metal ions are generally presented in environmental and biological samples. Consequently, the competition experiment was carried out to examine the binding ability of CNS toward other metal ions in THF/H<sub>2</sub>O (1 : 1, V/V) solution ( $1.0 \times 10^{-5}$  M). As shown in Fig. 4, the fluorescence intensity increased significantly after the addition of  $\text{Hg}^{2+}$ . In contrast, there were no obvious changes on the fluorescence intensity of CNS after

adding various metal ions, which proved again the high selectivity of probe CNS toward  $\text{Hg}^{2+}$ .

### 3.4 pH effects

Next, we studied the fluorescent intensity of probe CNS in the presence and absence of  $\text{Hg}^{2+}$  under different pH conditions (Fig. 5). In the absence of  $\text{Hg}^{2+}$ , the solution of probe CNS exhibited negligible fluorescence changes under a wide pH range,<sup>2-11</sup> which indicated its high stability under acidic and basic conditions. After addition of  $\text{Hg}^{2+}$ , the fluorescence intensity of probe CNS was significantly changed. However, the solution of probe CNS showed the maximum fluorescence intensity in the pH range from 3 to 8. This information revealed that probe CNS showed high stability and applicable to the biological scope.

Table 1 Comparison of CNS with other related fluorescent probes

Probe	LOD ( $\mu\text{M}$ )	pH range	Response time	Cell imaging	Zebrafish imaging	Ref.
	2.1	No data	No data	No	No	47
	4.42	4-8	No data	No	No	48
	1.65	No data	No data	No	No	49
	8	No data	6 min	Yes	No	50
	1.74/1.53	3-7.4	30 min	Yes	No	51
	9	No data	No data	Yes	No	39
	2.2	4-10	2 min	Yes	No	52
	2.78	3-8	45 s	Yes	Yes	This work



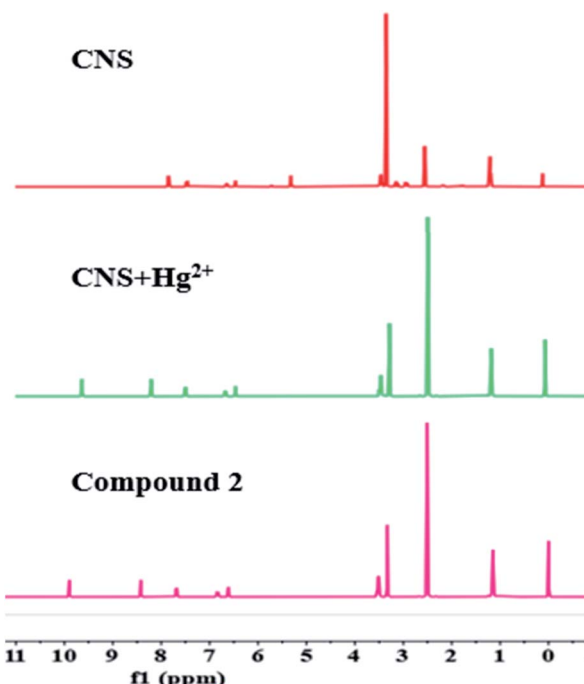
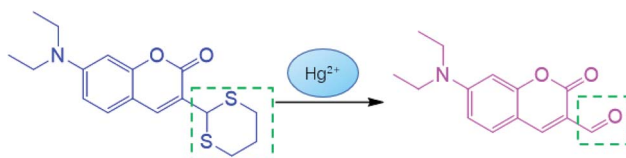


Fig. 7 The  $^1\text{H}$  NMR of CNS, CNS +  $\text{Hg}^{2+}$  and compound 2.



Scheme 2 Recognition mechanism of CNS for  $\text{Hg}^{2+}$ .

### 3.5 Response time of CNS

The response time of CNS to  $\text{Hg}^{2+}$  in THF/H<sub>2</sub>O solution (10<sup>-5</sup> M, 1 : 1, V/V) was investigated and the results were depicted in Fig. 6. Clearly, the fluorescence intensity of probe CNS reached its maximum in 1 minute and remained stable for 5 minutes after adding  $\text{Hg}^{2+}$ , demonstrating the fast responding time of CNS against  $\text{Hg}^{2+}$ .

Compared with other probes (Table 1), our probe has the fastest response time, and has a lower detection limit and a wider pH range. In terms of application, we have done cell experiments and zebrafish experiments, which fully demonstrates that our probe has a good application in biological detection.

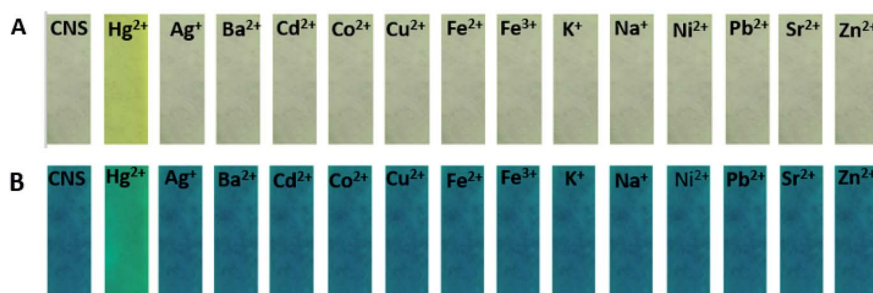


Fig. 8 The selectivity of the metal ions was tested with a filter paper, (A) in sunlight and (B) in UV light at 365 nm.

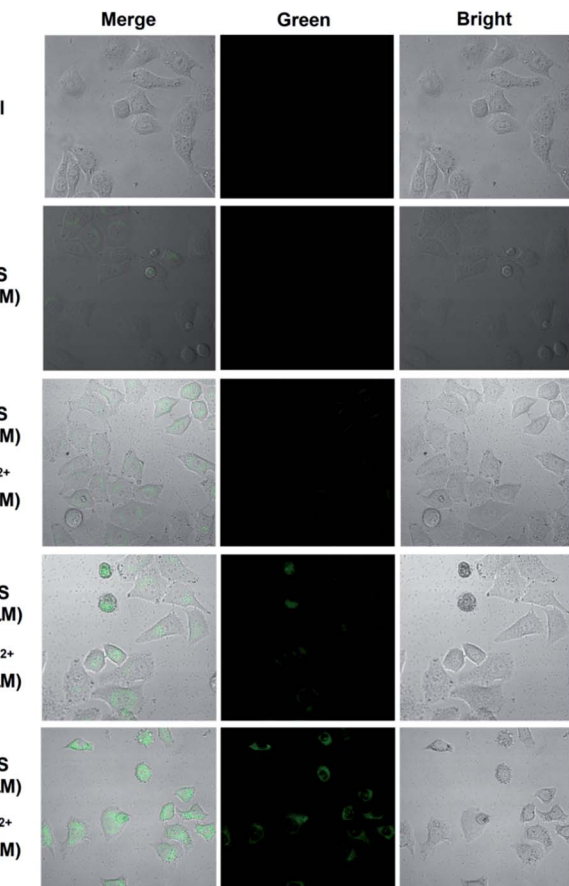


Fig. 9 Confocal fluorescence images of  $\text{Hg}^{2+}$  in living cells: cells incubated with CNS (10  $\mu\text{M}$ ) for 30 min; probe-loaded cells incubated with different concentrations of  $\text{Hg}^{2+}$  (10  $\mu\text{M}$ , 20  $\mu\text{M}$ , 50  $\mu\text{M}$ ) for 10 min. Then the fluorescence spectra were measured on a laser confocal microscopy. Green channel images: 490 nm–550 nm.

### 3.6 Detection mechanism

To investigate the proposed sensing mechanism of probe CNS for  $\text{Hg}^{2+}$ , we measured the  $^1\text{H}$  NMR spectra of probe CNS before and after reacting with  $\text{Hg}^{2+}$ . As shown in Fig. 7, after adding  $\text{Hg}^{2+}$  to the solution of CNS in  $\text{DMSO}-d_6$ , the original peaks at 3.48–3.27 and 3.23–3.12 ppm ascribed to the methylene protons of the thioacetal group disappeared, and a new peak at 9.65 ppm assigned to the aldehyde proton was observed. These results proved that the thioacetal group had been successfully



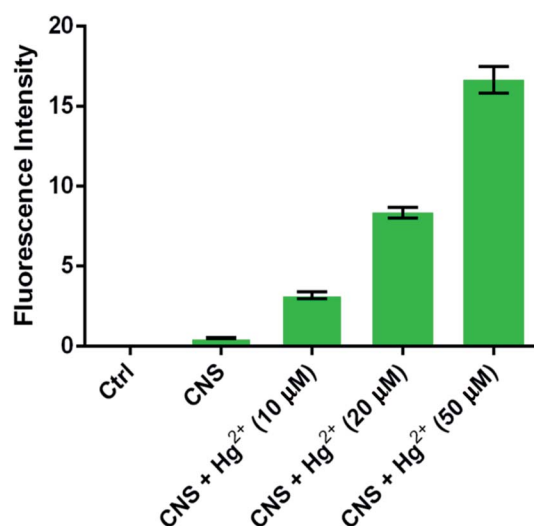


Fig. 10 The improvement of fluorescence intensities from HeLa cells (fluorescence intensity was analyzed by Image J software).

eliminated under the promotion of  $\text{Hg}^{2+}$ , which gave the corresponding aldehyde group and induced the intramolecular charge transfer (ICT) process, as shown in Scheme 2.

### 3.7 Paper test of probe CNS

A filter paper strip test was performed to study the convenience of probe CNS in practical application. Firstly, the filter paper was immersed in a probe solution (1.0 mM) and dried in air. Then the filter paper was immersed in a metal ion solution (1.0 mM). As shown in Fig. 8, the filter paper showed obvious color

change only under the induction of  $\text{Hg}^{2+}$ . The color change could be distinguished both under sunlight and 365 nm UV lamps. Therefore, the test bar can be used to test  $\text{Hg}^{2+}$  ion selectivity at any time.

### 3.8 Analytical applications in living cells

To investigate the biological applications of probe CNS, fluorescent imaging experiments were carried out in HeLa cells in the presence of 10  $\mu\text{M}$  probe CNS and different concentrations of  $\text{Hg}^{2+}$  (0, 10, 20, and 50  $\mu\text{M}$ ). As depicted in Fig. 9, HeLa cells treated with 10  $\mu\text{M}$  probe CNS for 30 min gave very weak fluorescence, which could be ascribed to the auto-fluorescence of probe CNS. To the medium was added 10  $\mu\text{M}$   $\text{Hg}^{2+}$  and the cells were incubated for 10 min, the fluorescence in HeLa cells were obviously improved, thereby indicating the chemical reaction between probe and  $\text{Hg}^{2+}$ . With the increasing of  $\text{Hg}^{2+}$  concentration (20  $\mu\text{M}$  and 50  $\mu\text{M}$ ), the fluorescence intensity in HeLa cells were significantly enhanced (Fig. 10). These results proved that CNS was a promising probe used for detecting  $\text{Hg}^{2+}$  in living cells, it could penetrate into HeLa cells in 30 min and rapidly respond to low concentrations of  $\text{Hg}^{2+}$ .

### 3.9 Toxicity of probe CNS in zebrafish

The toxicity of probe CNS was investigated in zebrafish larvae by measuring their behavioral tracks on an automated computerized video-tracking system (Fig. 11). Generally, high toxicity compound can dramatically affect the behavioral tracks of zebrafish larvae, including swimming duration, movement distance, and swimming speed. In our experiments, the zebrafish larvae treated with 5  $\mu\text{M}$  and 10  $\mu\text{M}$  probe CNS for 24 h, and

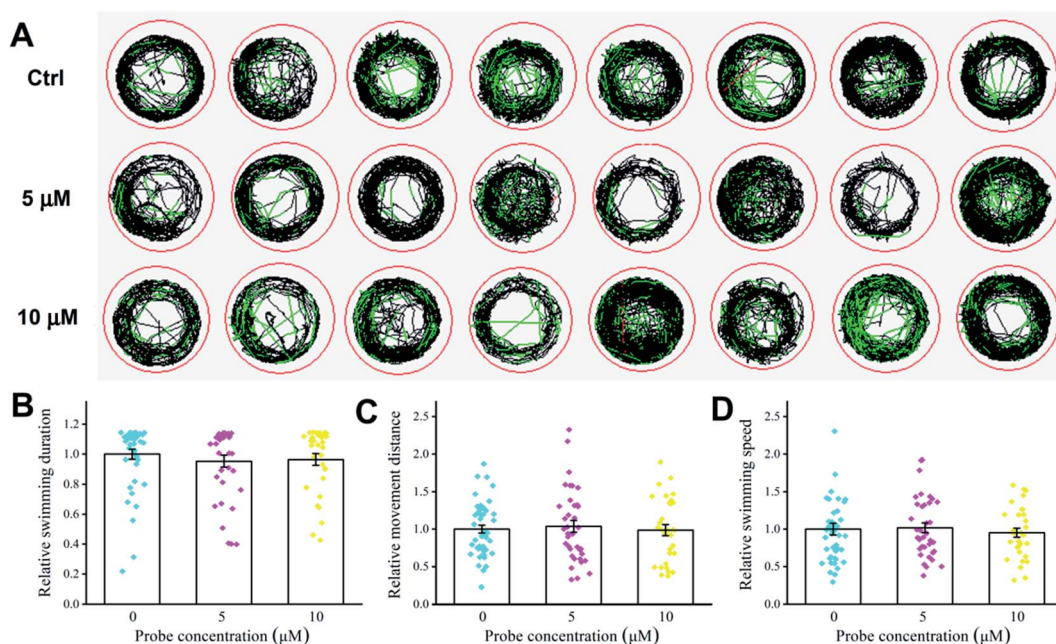


Fig. 11 Effect of different concentrations of CNS (0, 5, and 10  $\mu\text{M}$ ) on behavioral tracks of zebrafish. (A) Behavioral tracks. Red, green, and black lines depict fast, medium, and slow movement, respectively. (B) Swimming duration, (C) movement distance, and (D) swimming speed of zebrafish larvae.



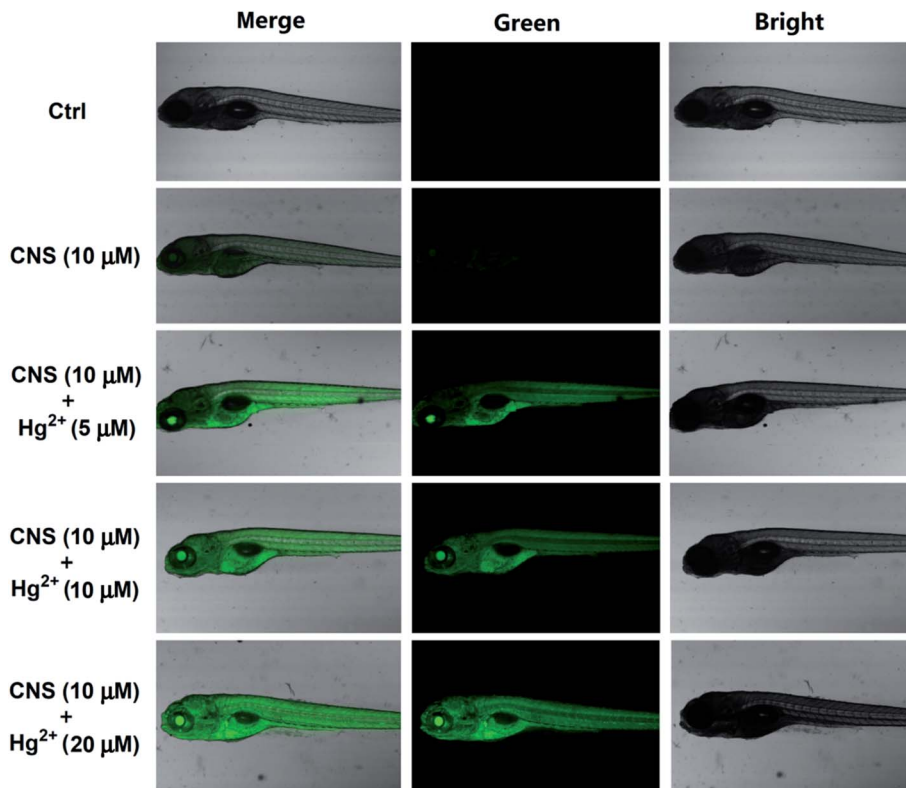


Fig. 12 Confocal fluorescence images of  $\text{Hg}^{2+}$  in zebrafish: zebrafish incubated with CNS (10  $\mu\text{M}$ ) for 30 min; probe-loaded zebrafish incubated with different concentrations of  $\text{Hg}^{2+}$  (5  $\mu\text{M}$ , 10  $\mu\text{M}$ , 20  $\mu\text{M}$ ) for 10 min. Then the fluorescence spectra were measured on a laser confocal microscopy. Green channel images: 490 nm–550 nm.

it seemed that probe **CNS** had no obvious effect on behavioral tracks of zebrafish larvae (Fig. 11A). There were no obvious decrease on the swimming duration (Fig. 11B), movement distance (Fig. 11C), and swimming speed (Fig. 11D). These data demonstrated that probe **CNS** exhibited very low toxicity at low concentrations.

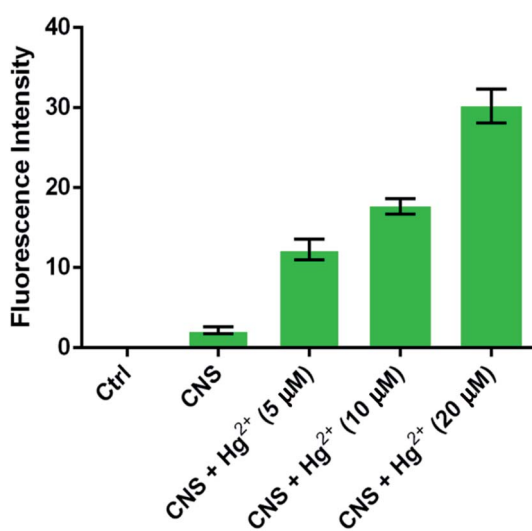


Fig. 13 The improvement of fluorescence intensities from zebrafish larvae (fluorescence intensity was analyzed by Image J software).

### 3.10 Analytical applications in zebrafish

We further investigated the biological applications of probe **CNS** in zebrafish before and after addition of difference concentrations of  $\text{Hg}^{2+}$ . The 5 days zebrafish larvae were incubated in E3 water containing 10  $\mu\text{M}$  probe **CNS** and different concentrations of  $\text{Hg}^{2+}$  (0, 5, 10, and 20  $\mu\text{M}$ ), then the fluorescence spectra were measured on a laser confocal microscopy. As shown in Fig. 12, the 5 days zebrafish larvae treated with E3 water containing 10  $\mu\text{M}$  probe **CNS** for 30 min emitted weak fluorescence generated by the probe itself. After incubation with 5  $\mu\text{M}$   $\text{Hg}^{2+}$  for 10 min, the zebrafish larvae gave strong green fluorescence improvement, and the fluorescence intensity was significantly enhanced with the increasing of  $\text{Hg}^{2+}$  concentration (Fig. 13). All these results indicated that probe **CNS** could be used for monitoring low concentrations of  $\text{Hg}^{2+}$  in living zebrafish model.

## 4. Conclusions

In summary, we have obtained a new coumarin-based colorimetric and fluorescent probe **CNS** by a low cost and high yield synthesis route. Probe **CNS** exhibited excellent selectivity and sensitivity, fast response time, as well as good stability under physiological pH condition. In filter paper strip test, an obvious color change could be observed upon addition of  $\text{Hg}^{2+}$ . The color change could be distinguished both under sunlight and 365 nm UV lamps, and the presence of other competitive metal



ions had no obvious interference on the background. The probe showed low toxicity to zebrafish larvae, and was successfully used for detecting increasing concentrations of  $Hg^{2+}$  in HeLa cells and zebrafish model. All these results indicated that probe CNS should be a promising fluorescent agent for detecting  $Hg^{2+}$  in environmental samples and living biological systems.

## Ethical statement

Animal procedures were conducted in compliance with the NIH Guide for the Care and Use of Laboratory Animals (No.8023, amended in 1996), and approved by the Animal Care and Use Committee of Qilu University of Technology that followed the guideline for the Care and Use of Laboratory Animals of China.

## Conflicts of interest

The authors declare no competing financial interests.

## Acknowledgements

This work was supported by the Key Research and Development Program of Shandong Province of China (2018 CXGC1106), and Young Science Foundation of Shandong Academy of Sciences (No. 2020QN0018).

## References

- 1 B. Zhou, S. Qin, B. Chen and Y. Han, A new BODIPY-based fluorescent “turn-on” probe for highly selective and rapid detection of mercury ions, *Tetrahedron Lett.*, 2018, **59**(49), 4359–4363.
- 2 S. Koenig, M. Solé, C. Fernández-Gómez and S. Díez, New insights into mercury bioaccumulation in deep-sea organisms from the NW Mediterranean and their human health implications, *Sci. Total Environ.*, 2013, **442**, 329–335.
- 3 H. Li, J. Zhai, J. Tian, Y. Luo and X. Sun, Carbon nanoparticle for highly sensitive and selective fluorescent detection of mercury(II) ion in aqueous solution, *Biosens. Bioelectron.*, 2011, **26**(12), 4656–4660.
- 4 H. Xiao, J. Li, K. Wu, G. Yin, Y. Quan and R. Wang, A turn-on BODIPY-based fluorescent probe for  $Hg^{(II)}$  and its biological applications, *Sens. Actuators, B*, 2015, **213**, 343–350.
- 5 R. Zou, X. Zeng, G. Luo, Y. Qiu, B. Zhang, Y. Xu, *et al.*, Mercury stability of byproducts from wet flue gas desulfurization devices, *Fuel*, 2016, **186**, 215–221.
- 6 H. Xu, Y. Ma, W. Huang, J. Mei, S. Zhao, Z. Qu, *et al.*, Stabilization of mercury over Mn-based oxides: speciation and reactivity by temperature programmed desorption analysis, *J. Hazard. Mater.*, 2017, **321**, 745–752.
- 7 Y. Zhou, X. He, H. Chen, Y. Wang, S. Xiao, N. Zhang, *et al.*, An ESIPT/ICT modulation based ratiometric fluorescent probe for sensitive and selective sensing  $Hg^{2+}$ , *Sens. Actuators, B*, 2017, **247**, 626–631.
- 8 J. Vas and M. Monestier, Immunology of Mercury, *Ann. N. Y. Acad. Sci.*, 2008, **1143**(1), 240–267.
- 9 A. Masih, A. Taneja and R. Singhvi, Exposure profiles of mercury in human hair at a Terai belt of North India, *Environ. Geochem. Health*, 2016, **38**(1), 145–156.
- 10 C. Song, B. Yang, Y. Zhu, Y. Yang and L. Wang, Ultrasensitive silver nanorods array SERS sensor for mercury ions, *Biosens. Bioelectron.*, 2017, **87**, 59–65.
- 11 W. Crowe, P. J. Allsopp, G. E. Watson, P. J. Magee, J. J. Strain, D. J. Armstrong, *et al.*, Mercury as an environmental stimulus in the development of autoimmunity – a systematic review, *Autoimmun. Rev.*, 2017, **16**(1), 72–80.
- 12 E. M. Nolan and S. J. Lippard, Tools and Tactics for the Optical Detection of Mercuric Ion, *Chem. Rev.*, 2008, **108**(9), 3443–3480.
- 13 D. W. Boening, Ecological effects, transport, and fate of mercury: a general review, *Chemosphere*, 2000, **40**(12), 1335–1351.
- 14 C. Wu, J. Wang, J. Shen, C. Bi and H. Zhou, Coumarin-based  $Hg^{2+}$  fluorescent probe: synthesis and turn-on fluorescence detection in neat aqueous solution, *Sens. Actuators, B*, 2017, **243**, 678–683.
- 15 J. V. Cizdziel and S. Gerstenberger, Determination of total mercury in human hair and animal fur by combustion atomic absorption spectrometry, *Talanta*, 2004, **64**(4), 918–921.
- 16 A. Q. Shah, T. G. Kazi, J. A. Baig, H. I. Afridi and M. B. Arain, Simultaneously determination of methyl and inorganic mercury in fish species by cold vapour generation atomic absorption spectrometry, *Food Chem.*, 2012, **134**(4), 2345–2349.
- 17 Y. Zhao, J. Zheng, L. Fang, Q. Lin, Y. Wu, Z. Xue, *et al.*, Speciation analysis of mercury in natural water and fish samples by using capillary electrophoresis-inductively coupled plasma mass spectrometry, *Talanta*, 2012, **89**, 280–285.
- 18 O. Abollino, A. Giacomino, M. Malandrino, G. Piscionieri and E. Mentasti, Determination of Mercury by Anodic Stripping Voltammetry with a Gold Nanoparticle-Modified Glassy Carbon Electrode, *Electroanalysis*, 2008, **20**(1), 75–83.
- 19 K. Ponnuvel, V. Padmini and R. Sribalan, A new tetrazole based turn-on fluorescence chemosensor for  $Zn^{2+}$  ions and its application in bioimaging, *Sens. Actuators, B*, 2016, **222**, 605–611.
- 20 K. Ponnuvel, M. Kumar and V. Padmini, A new quinoline-based chemosensor for  $Zn^{2+}$  ions and their application in living cell imaging, *Sens. Actuators, B*, 2016, **227**, 242–247.
- 21 B. Zhu, Z. Wang, Z. Zhao, W. Shu, M. Zhang, L. Wu, *et al.*, A simple highly selective and sensitive hydroquinone-based two-photon fluorescent probe for imaging peroxynitrite in live cells, *Sens. Actuators, B*, 2018, **262**, 380–385.
- 22 L. Wang, J. Zhang, X. An and H. Duan, Recent progress on the organic and metal complex-based fluorescent probes for monitoring nitric oxide in living biological systems, *Org. Biomol. Chem.*, 2020, **18**(8), 1522–1549.
- 23 H. N. Kim, W. X. Ren, J. S. Kim and J. Yoon, Fluorescent and colorimetric sensors for detection of lead, cadmium, and mercury ions, *Chem. Soc. Rev.*, 2012, **41**(8), 3210–3244.
- 24 J. F. Zhang, Y. Zhou, J. Yoon and J. S. Kim, Recent progress in fluorescent and colorimetric chemosensors for detection of precious metal ions (silver, gold and platinum ions), *Chem. Soc. Rev.*, 2011, **40**(7), 3416–3429.



25 S.-L. Kao and S.-P. Wu, A fluorescent turn-on probe for  $\text{Hg}^{(\text{II})}$  based on an  $\text{NTe}_2$  chelating motif and its application in living cell imaging, *Sens. Actuators, B*, 2015, **212**, 382–388.

26 S. Erdemir, O. Kocigit and S. Karakurt, A new perylene bisimide-armed calix[4]-aza-crown as “turn on” fluorescent sensor for  $\text{Hg}^{2+}$  ion and its application to living cells, *Sens. Actuators, B*, 2015, **220**, 381–388.

27 S.-Y. Yu and S.-P. Wu, A highly selective turn-on fluorescence chemosensor for  $\text{Hg}^{(\text{II})}$  and its application in living cell imaging, *Sens. Actuators, B*, 2014, **201**, 25–30.

28 K. M. Vengaian, C. D. Britto, K. Sekar, G. Sivaraman and S. Singaravelivel, Fluorescence “on-off-on” chemosensor for selective detection of  $\text{Hg}^{2+}$  and  $\text{S}_2^-$ : application to bioimaging in living cells, *RSC Adv.*, 2016, **6**(9), 7668–7673.

29 A. K. Jha, S. Umar, R. K. Arya, D. Datta and A. Goel, Pyrano [3,2-*c*]ulolidin-2-ones: a novel class of fluorescent probes for ratiometric detection and imaging of  $\text{Hg}^{2+}$  in live cancer cells, *J. Mater. Chem. B*, 2016, **4**(28), 4934–4940.

30 K. M. Vengaian, C. D. Britto, G. Sivaraman, K. Sekar and S. Singaravelivel, Phenothiazine based sensor for naked-eye detection and bioimaging of  $\text{Hg}^{(\text{II})}$  and  $\text{F}^-$  ions, *RSC Adv.*, 2015, **5**(115), 94903–94908.

31 J. Ding, H. Li, C. Wang, J. Yang, Y. Xie, Q. Peng, *et al.*, “Turn-On” Fluorescent Probe for Mercury( $\text{II}$ ): High Selectivity and Sensitivity and New Design Approach by the Adjustment of the  $\pi$ -Bridge, *ACS Appl. Mater. Interfaces*, 2015, **7**(21), 11369–11376.

32 Y. Yan, Y. Zhang and H. Xu, A Selective “Turn-On” Fluorescent Probe for Recognition of Mercury( $\text{II}$ ) Ions in Aqueous Solution Based on a Desulfurization Reaction, *ChemPlusChem*, 2013, **78**(7), 628–631.

33 M. Santra, B. Roy and K. H. Ahn, A “Reactive” Ratiometric Fluorescent Probe for Mercury Species, *Org. Lett.*, 2011, **13**(13), 3422–3425.

34 F. Borges, F. Roleira, N. Milhazes, L. Santana and E. Uriarte, Simple Coumarins and Analogues in Medicinal Chemistry: Occurrence, Synthesis and Biological Activity, *Curr. Med. Chem.*, 2005, **12**(8), 887–916.

35 X.-y. Sun, T. Liu, J. Sun and X.-j. Wang, Synthesis and application of coumarin fluorescence probes, *RSC Adv.*, 2020, **10**(18), 10826–10847.

36 M. Xing, K. Wang, X. Wu, S. Ma, D. Cao, R. Guan, *et al.*, A coumarin chalcone ratiometric fluorescent probe for hydrazine based on deprotection, addition and subsequent cyclization mechanism, *Chem. Commun.*, 2019, **55**(99), 14980–14983.

37 M. E. Aliaga, M. Gazitua, A. Rojas-Bolanos, M. Fuentes-Estrada, D. Durango and O. Garcia-Beltran, A selective thioxothiazolidin-coumarin probe for  $\text{Hg}^{2+}$  based on its desulfurization reaction. Exploring its potential for live cell imaging, *Spectrochim. Acta, Part A*, 2020, **224**, 7.

38 C. G. Chen, N. Vijay, N. Thirumalaivasan, S. Velmathi and S. P. Wu, Coumarin-based  $\text{Hg}^{2+}$  fluorescent probe: fluorescence turn-on detection for  $\text{Hg}^{2+}$  bioimaging in living cells and zebrafish, *Spectrochim. Acta, Part A*, 2019, **219**, 135–140.

39 X. H. Cheng, S. H. Qu, L. Xiao, W. N. Li and P. He, Thioacetalized coumarin-based fluorescent probe for mercury( $\text{II}$ ): ratiometric response, high selectivity and successful bioimaging application, *J. Photochem. Photobiol., A*, 2018, **364**, 503–509.

40 Y. Ding, Y. M. Pan and Y. F. Han, A Coumarin-Based Fluorescent Probe for Ratiometric Monitoring of  $\text{Hg}^{2+}$  in Live Cells, *Ind. Eng. Chem. Res.*, 2019, **58**(19), 7786–7793.

41 M. Dong, J. Y. Tang, Y. F. Lv, Y. T. Liu, J. F. Wang, T. T. Wang, *et al.*, A dual-function fluorescent probe for  $\text{Hg}^{(\text{II})}$  and  $\text{Cu}^{(\text{II})}$  ions with two mutually independent sensing pathways and its logic gate behavior, *Spectrochim. Acta, Part A*, 2020, **226**, 7.

42 X. W. Li, Q. X. Duan, Y. M. Yu, K. Wang, H. C. Zhu, X. Zhang, *et al.*, A coumarin-based fluorescent probe for  $\text{Hg}^{2+}$  and its application in living cells and zebrafish, *Luminescence*, 2020, **35**(6), 941–946.

43 S. Mondal, N. Patra, H. P. Nayek, S. K. Hira, S. Chatterjee and S. Dey, Unusual absence of FRET in triazole bridged coumarin-hydroxyquinoline, an active sensor for  $\text{Hg}^{2+}$  detection, *Photochem. Photobiol. Sci.*, 2020, **19**(9), 1211–1221.

44 J. M. V. Ngororabanga, Z. R. Tshentu and N. Mama, A New Highly Selective Colorimetric and Fluorometric Coumarin-based Chemosensor for  $\text{Hg}^{2+}$ , *J. Fluoresc.*, 2020, **30**(5), 985–997.

45 Z. X. Pan, Z. X. Xu, J. Chen, L. P. Hu, H. Q. Li, X. Zhang, *et al.*, Coumarin Thiourea-Based Fluorescent Turn-on  $\text{Hg}^{2+}$  Probe That Can Be Utilized in a Broad pH Range 1–11, *J. Fluoresc.*, 2020, **30**(3), 505–514.

46 Y. M. Yu, C. Y. Liu, B. Tian, X. Y. Cai, H. C. Zhu, P. Jia, *et al.*, A novel highly selective ratiometric fluorescent probe with large emission shift for detecting mercury ions in living cells and zebrafish, *Dyes Pigm.*, 2020, **177**, 7.

47 H. E. Jiang, D. N. Tang, Z. J. Li, J. W. Li, H. B. Liu, Q. J. Meng, *et al.*, A dual-channel chemosensor based on 8-hydroxyquinoline for fluorescent detection of  $\text{Hg}^{2+}$  and colorimetric recognition of  $\text{Cu}^{2+}$ , *Spectrochim. Acta, Part A*, 2020, **243**, 6.

48 L. N. Liu, L. He, Y. Qu, N. Lu, Q. Y. Cao and Z. H. Yan, A hydroxyquinoline-base nanoprobe for fluorescent sensing of  $\text{Hg}^{2+}$  ion in aqueous solution, *Inorg. Chim. Acta*, 2018, **474**, 128–133.

49 C. M. Lopez-Alled, L. C. Murfin, G. Kociok-Kohn, T. D. James, J. Wenk and S. E. Lewis, Colorimetric detection of  $\text{Hg}^{2+}$  with an azulene-containing chemodosimeter via dithioacetal hydrolysis, *Analyst*, 2020, **145**(19), 6262–6269.

50 J. Ding, H. Y. Li, C. Wang, J. Yang, Y. J. Xie, Q. Peng, *et al.*, “Turn-On” Fluorescent Probe for Mercury( $\text{II}$ ): High Selectivity and Sensitivity and New Design Approach by the Adjustment of the  $\pi$ -Bridge, *ACS Appl. Mater. Interfaces*, 2015, **7**(21), 11369–11376.

51 Y. Y. Gao, T. T. Ma, Z. Z. Ou, W. J. Cai, G. Q. Yang, Y. Li, *et al.*, Highly sensitive and selective turn-on fluorescent chemosensors for  $\text{Hg}^{2+}$  based on thioacetal modified pyrene, *Talanta*, 2018, **178**, 663–669.

52 M. S. Xu, L. Wang, M. Li, Z. W. Ma, D. Zhang and J. H. Liu, A new highly sensitive and selective fluorescent probe for  $\text{Hg}^{2+}$  and its application in living cells, *Phosphorus, Sulfur Silicon Relat. Elem.*, 2020, **196**(1), 13–18.

